INVESTIGATIONS OF RF NOISE INTRODUCED BY PHOTOVOLTAIC SOLAR POWER GENERATORS

M. Drapalik[1)], V. Schlosser[1)], J. Schmid[1)], P. Bajons[2)], G. Klinger[3)]
1. Department of Electronic Properties of Materials, Faculty of Physics, University of Vienna
2. Department of Scattering and Spectroscopy, Faculty of Physics, University of Vienna
3. Department of Meteorology and Geophysics, University of Vienna
A-1090 Vienna, Austria

ABSTRACT: We have investigated the a.c. behaviour of crystalline silicon solar cells with abrupt *pn*-junction doping profiles. From small signal admittance measurements we derived the complex impedance of the solar cell. The low frequency transfer function up to 1MHz was determined by modelling the circuit of the solar cell connected to an external impedance. Under laboratory conditions we examined the current response of the solar cells connected to an external impedance caused by periodic light intensity variations or mechanical vibrations with respect to our model calculations. We found that the investigated solar cells act as a low pass filter in the external current loop with a bias voltage dependent bandwidth which can exceed 100 kHz.
Keywords: Electromagnetic Compatibility – Silicon Solar Cell - Impedance

1 INTRODUCTION

The installation of an electrical power generator with a capacity of 1 MW_p based on solar cell technology requires an area of approximately 7000 m^2 occupied by photovoltaic arrays. Beside the useful d.c. current output of the arrays several noise sources generate additional transient current components which are transmitted to the power conditioning unit or emitted to the ambience. Without precautions the overall level of electromagnetic interference in the surroundings of PV installations

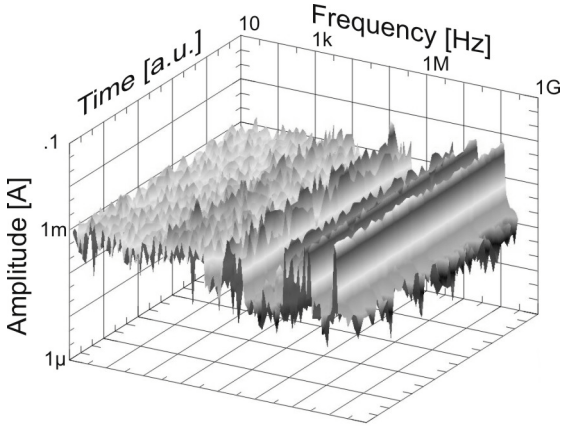

Figure 1: Noise spectra measured at the terminals of a 10 W solar panel which was mounted on the roof top of the institute in central Vienna. The spectra were sampled for approx. 1 hour on a clear sunny day.

therefore can increase to an intolerable high value [1-3]. The origin of the distortion currents can be internal noise of the semiconducting devices [4] light fluctuations, received RF signals and mechanical vibrations of the modules. An example of the spectral analysis of electrical noise present at the terminals of a 10 W_p module mounted at the roof top of the institute in central Vienna is shown in fig.1. The analysed frequencies ranged from 10 Hz to 1 GHz. Beside several narrow frequency bands arising from the reception of RF signals a continuous spectrum of current amplitudes below 1 MHz was observed. The level varied somewhat with incident light intensity. At windy conditions amplitudes below 1 kHz increases and below 100 Hz vibrations sometimes became the major contribution to the noise spectra.

The content of our current investigations concerns the study of the signal response of single solar cells made from crystalline silicon under well controlled laboratory conditions. It includes measurements and modelling of the a.c. properties of the cells below 1MHz, Light excitation with pulsed or sinusoidal intensity modulated sources, the determination of the response function to RF radiation up to 4 GHz and the observation of signal amplitudes caused by vibrations in the low frequency regime. In this contribution we present some exemplary results from our investigations in order to illustrate the different aspects of noise generation and transmission rather than to present a detailed analysis.

2 EXPERIMENTAL

2.1 Equivalent a.c. circuit model

The dimensions of the solar cell together with the front metal grid design mainly determine the high frequency behaviour for electromagnetic signals with wavelengths comparable to the cell's physical sizes – length, width, thickness –. The cell's response to lower frequency signals is governed by the properties of the semiconducting material and the cell's architecture. The presented transient circuit model follow the approach given in [4] which appears to be appropriate for modelling the low frequency response of a one sided abrupt planar *pn*-junction in crystalline silicon. It was extended by an inductor in series with an external load resistor in order to account for the inductance arising from the front metal grid. The photovoltaic carrier generation can be modelled by a current source which introduces the light generated current I_{ph} into the circuit which consists of three internal and one external current loop given by:

1. a voltage dependent capacitor, C_{tot}.
2. a shunt resistor, R_{sh}.
3. a dynamic resistance, R_0 determined by the diode characteristics of the current voltage dependence.
4. the externally connected Impedance Z_L.

For the calculation of the partial currents it is more convenient to use the complex admittance rather than the

impedance. The complex admittance $i\omega C_{tot}$ summarises two capacitors in parallel, namely the depletion capacitance C_{depl} which dominates under reverse bias voltage conditions and the diffusion capacitance C_{diff} which exponentially increases with forward voltages. The angular frequency is defined by $\omega=2\pi\nu$ where ν is the frequency and i is the imaginary unit (i^2=-1). The shunt conductance is defined by $G_{sh}=R_{sh}^{-1}$. $G_0=R_0^{-1}$ mathematically is obtained from the first derivative of the current voltage relation:

$$G_0 = \frac{\partial I}{\partial V} = I_0 \frac{q}{nk_BT} \cdot \exp\left(\frac{qV}{nk_BT}\right) \quad (1)$$

Where the diode saturation current is expressed by I_0, q is the elementary charge, k_B the Boltzmann constant, n the diode factor and T the absolute temperature. The admittance at low frequencies due to the diffusion of carriers can be approximated by [4]:

$$Y_{diff} = G_0 \cdot \left(1 + i\frac{\omega\tau_{transit}}{2}\right) \quad (2)$$

For an abrupt junction profile in *p*-Si the transit time $\tau_{transit}$ equals the electron lifetime τ_n in the *p*-type base region. Except for C_{depl} and $\tau_{transit}$ all information to calculate the internal admittance of the solar cell can be derived from the static $I(V)$ relation.

Beside the electronic component(s) connected to the terminals of the solar cell and characterised by a load admittance Z_L^{-1} the internal resistive and inductive losses, R_S and L_{grid} at the metal contacts determine magnitude and phase of the experimentally accessible current in the circuit. The complex ratio of the external to the internal current loops determine the bandwidth and the transfer function at the terminals of the solar cell.

2.2 Small signal measurements

From small signal measurements both the static $I(V)$ relation and the real and imaginary part of the admittance were derived. The solar cell was connected to a voltage source in series with an inductance free resistor of 50 Ω which is used as current shunt. The variable d.c. voltage V_{DC} was superimposed by a sinusoidal a.c. voltage of approx. 15 mV_{rms} at ν=4.3 kHz. In our experiments V_{DC} was varied between –1.5 V and +0.5 V. The bias voltage and the shunt voltage were recorded with an oscilloscope and Fourier transformed. The d.c. offsets of the 2 signals were used to determine the static $I(V_{DC})$ characteristic. The magnitude and phase difference of the first harmonics were used to derive the area normalised internal cell conductance $g_{int}=(G_{sh}+G_0)/A$ and the capacitance $c_{tot}=C_{tot}/A$. A is the total area of the solar cell. The static $I(V)$ curve was numerically derived in order to obtain $g_{int}(\nu=0)$ and compared with the direct determination of $g_{int}(\nu>0)$ from the small signal measurement. Once the measurement frequency is sufficiently low and the a.c. amplitude small both sets of data for g_{int} should be identical verifying that the experimental settings were properly chosen and the experiment is in accordance with the assumed a.c. circuit model. Below V_{DC}<0V g_{int} becomes constant and is determined by g_{sh}. Since for V_{DC}<0V C_{diff} becomes negligible the experimentally obtained $c_{tot}(V_{DC}<0\text{ V})\approx c_{depl}$ was used to fit $c_{depl}(V_{DC})$ assuming a linear variation with $(V_{bi}-V)^{-1/2}$ [5]. A high correlation of the linear dependency verifies that the assumption of an abrupt doping profile is justified. From slope and intercept the build in voltage, V_{bi} and the background concentration, N_{base} can be derived. From the knowledge of c_{depl} the diffusion capacitance c_{diff} can be obtained by subtraction. Equation 2 shows that c_{diff} should scale with g_0 with a factor of $\tau_{transit}/2$. Since $\tau_{transit}$ was not experimentally determined it was assumed in such a way that the model calculations fit best to the experimentally observed data for c_{diff}. An example of the evaluation of the cell's admittance from small signal measurements is shown in fig.2. The cell under investigation was a 15.63cm^2 large

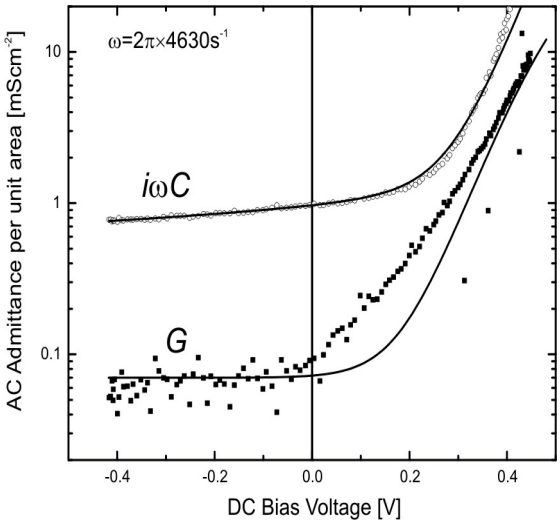

Figure 2: Comparison of the experimentally observed (symbols) and from model calculations derived (line) admittance of a *pn*-junction solar cell.

multicrystalline silicon cell.

2.3 Light modulation measurements

A sinusoidal light excitation in the frequency range between 5 Hz and 1 MHz was applied to the solar cell under test. The light source was a high power, fast switching ($\tau_{rise}<\tau_{fall}$<20 ns) IR LED with a peak intensity at 870 nm. The emitted light intensity varies almost linear with the LED current. An inductance free 1 Ω shunt re-

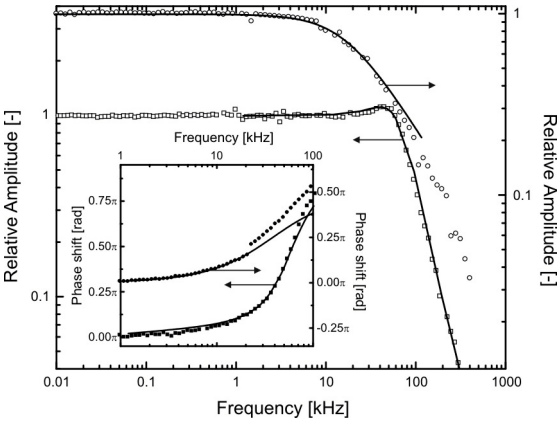

Figure 3: Experimentally derived (symbols) and calculated (lines) amplitude attenuation of a mc-Si solar cell. The inset show the phase shift. Squares are measurements with a voltage source, circles indicate that the external resistor was directly connected to the cell.

sistor alone or in series with a voltage source was connected to the terminals of the solar cell. The LED current and the cell's current response picked up at the shunt resistor were monitored with an oscilloscope. The frequency dependence of the signal response was derived from the experimental recordings. Due to the variation of c_{tot} and g_{int} with V_{DC} the transfer function varies with working point of the photovoltaic device. Therefore the experiments were repeated for several bias voltages either forced by the voltage source in the reverse and forward regime of the diode or by applying a constant white background illumination. As assumed from the model the signal response essentially is determined by a low pass characteristic. Depending whether the voltage source was present in the outer current loop or not the characteristic significantly differs indicating that the voltage source adds a complex impedance to the external load. An example of the experimentally obtained current transfer characteristic at V_{DC}=0V is shown in fig.3 together with calculations from the equivalent circuit model.

2.4 Vibration measurements

Photovoltaic arrays are exposed to wind forces which can introduce mechanical vibrations. These vibrations cause changes of the module's surface orientation with respect to the incident sun light described by an angle of misorientation, Θ, which can vary between 0 and π/2. In the first case the module's surface is oriented perpendicular to the direction of the sun rays in the letter it is oriented parallel. Thus the effective cell area exposed perpendicular to the incident sun rays varies with cos Θ. In our experiments a single crystal silicon solar cell of a size of approximately $2\,\text{cm} \times 5\,\text{cm}$ was mounted on a three axis vibration table in a vertical position. The cell was illuminated by a halogen lamp unit with a focusing mirror which emits a narrow light beam. The angle of misorientation determined by the cell's surface vector and the optical axis of the light source was arranged in a horizontal plane and varied between 0 and 1.2 rad. The vertical Z-axis of the vibration table was displaced sinusoidal at a frequency of 16.94 Hz without any additional excitation of the horizontal X and Y axis. The frequency was chosen close to the resonant condition of our set up which was found at 12.9 Hz. The first harmonic of the a.c. current normalised to the d.c. current of the solar cell was recorded as a function of the amplitude of displacement which was controlled in the range between 0 µm and 500 µm peak to peak. The result for three values of Θ is shown in fig.4.

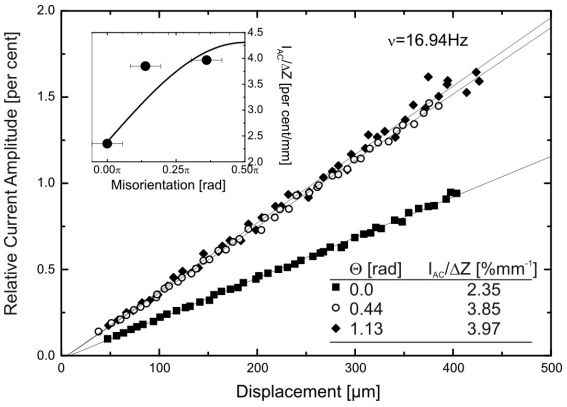

Figure 4: Observed current oscillations caused by mechanical vibrations of a crystalline silicon solar cell.

3 RESULTS AND DISCUSSION

The transfer function of the investigated solar cell under various conditions could be found analytically once all internal elements of the circuit are determined and the external components are known. Beside the externally connected load cable losses and wiring contribute to the total impedance. Therefore we preferentially evaluated the signal response by simulation using either the program Multisim [6] or Qucs [7] which allowed us to easily vary the real and imaginary components of the external current branch in order to adapt the model calculations to the experimentally observed frequency response. In the absence of a voltage source the external path was determined by an inductance free resistor of known magnitude which was connected to the terminals of the solar cell in order to monitor the external current. In series with this current shunt resistor an additional resistive component and an inductor has to be introduced in the simulations. Physically the ohmic element represents the sum of the cell's internal series resistance and wiring or connection losses introduced by our experimental set up. The inductive element mainly arises from the inductance of the front surface grid. However the external wiring of the cell may contribute as well which could not be extracted from the experimental results or from the simulation. The use of the voltage source added 1.6 Ω and 96 µH to the external impedance. With one set of lumped elements the simulation described fairly well both modulated light intensity and pulsed light measurements at various bias voltages and different white bias light levels. Nevertheless deviations were observed towards elevated frequencies as can be seen in fig.3. They are potentially caused by additional surface and interface currents which are not considered in the present model. In the experiments the solar cell's d.c. current was restricted to values which could be compensated at the oscilloscope's channel input. This limits the application of the bias light to intensities of less than $100\,\text{Wm}^{-2}$. Therefore we could not observe experimentally the frequency response at working points of the solar cell when operated at high levels of incident light intensities. For low intensities we have not found that a change of the background illumination changes the solar cell's small signal admittance. Therefore once the results of model calculations and experimental data agree sufficiently well we used the model parameters to extrapolate the calculations of the transfer function to the case of high incident irradiation. In table 1 the results of the experimentally observed and the calculated frequency response of the a.c. current derived for a multicrystalline silicon solar cell with an area of $15.63\,\text{cm}^2$ are summarised. For the calculation an incident light intensity of $1000\,\text{Wm}^{-2}$ resulting in a short circuit current density of $300\,\text{Am}^{-2}$ was assumed. The calculated parameters are given for the bias condition of maximum power output of the solar cell. Cell capacitance and resistance are taken from the results of the small signal measurements. The inductance introduced by the grid is assumed to be independent from bias voltage. The matched external load is assumed to be merely resistive and was determined by the cell's current-

voltage dependence under illumination. The condition that the current amplitude is attenuated by -3 dB with respect of its initial low frequency magnitude defines the bandwidth. The slope of the linear decrease of the amplitudes at high frequencies in the double logarithmic plot specify the attenuation of the low pass filter.

Table I: Summarised a.c. response of a mc Si solar cell.

Parameter	Experiment	Calculation	Unit
DC Bias Voltage	0.0	0.48	V
Cell Capacitance	32.5	406	$nFcm^{-2}$
Cell Resistance	12.9	0.083	$k\Omega cm^2$
Cell Inductance	50	50	μHcm^2
Load Resistance	54.4	20.2	Ωcm^2
Bandwidth	126	31	kHz
Attenuation	-11.2	-10.8	dB/Oct.

Light intensity fluctuations occur in a wide frequency range and therefore can become a significant source of current noise in a photovoltaic system. Beside the direct conversion of light noise to current noise in the low frequency regime dumped current oscillations invoked by spikes and demodulation effects of the rectifier can increase the overall current noise level introduced by the incident light.

We have found that periodic mechanical vibrations generate current oscillations as can be seen in fig.4. For small excitations the current amplitude varies linearly with the cell's displacement in one direction. The resulting amplitudes can become even larger than 1 per cent of the total light generated d.c. current. Since the derivative of the angular dependence of the induced current is expected to vary with $\sin\Theta$ it should vanish for perpendicular light incidence and be largest for the case of parallel incidence. Experimentally we observed the smallest current amplitudes for $\Theta = 0$ rad (perpendicular incidence) which rapidly increase with the angle of misorientation. The differences between the expected and experimentally determined angular dependence can primarily be explained by the beam divergence of the light source in our experiments. The large error bars for Θ shown in the inset of fig.4 reflects this circumstance. A more refined evaluation of our results however would require the application of a distribution of Θ rather than simply using the optical axis to define a single angle of misorientation.

From the investigations we have made so far it can be assumed that mechanical vibrations are capable to generate significant large noise currents especially at low frequencies. However the probability that noise currents exceed 1 per cent during the daily operation of a solar power generator is rather small since several conditions have to coincide: (i) direct sun light must be dominant and at the same time the angle of misorientation has to be large. For fixed mounted photovoltaic arrays this is most likely in the morning or evening hours. (ii) wind forces has to stimulate mechanical vibrations close to the resonance frequency of the array construction.

4 CONCLUSIONS

A photovoltaic solar cell connected to an external load basically act as an electronic low pass filter for a.c. currents which can be modelled by lumped electronic components. The frequency response of the current amplitudes depends on the working point and on the complex impedance of the external load. For crystalline silicon solar cells with an abrupt *pn*-junction doping profile all parameters necessary to model the transfer function sufficiently well can be derived from static current-voltage and small signal admittance measurements at low frequencies. The low pass bandwidth can exceed 30 kHz when the solar cells are operated at the working point of maximum power output. The cut off frequency is independent of the cell area. Beside the reception of electromagnetic noise emitted from a variety of sources light fluctuations and mechanical vibrations can introduce current noise into the circuit.

References

[1] Wada, T., Mori, T., Tokuda, M., Suenaga, S., Igarashi, H., Proc. of the International Symposium on EMC, 2005, **1**, 112.

[2] Di Piazza, M. C., Serporta, C., Tinè, G., Vitale, G., Proc. of IEEE International Conference on Industrial Technology, 2004, **2**, 672.

[3] Igarachi, H., Suenaga, S., Proc. of the 31st IEEE Photovoltaic Specialist Conference, 2005, 1820.

[4] Mallette, L. A., Phillips, R. L., Appl. Optics, 1978, **17**, 1780.

[5] Müller, R. Grundlagen der Halbleiter-Elektronik, Halbleiter-Elektronik 1, W. Heywang and R. Müller Ed., Springer, Berlin 1979, 136.

[6] http://www.ni.com/multisim/

[7] http://qucs.sourceforge.net/